Individual tree species classification from airborne multi-sensor imagery using robust PCA

Juheon Lee[a,b], Xiaohao Cai[a,b,g], Jan Lellmann[b], Michele Dalponte[a,c], Yadvinder Malhi[d], Nathalie Butt[d,e], Mike Morecroft[f], Carola-Bibiane Schönlieb[b], and David A. Coomes[a]

[a]Forest Ecology and Conservation Group, Department of Plant Sciences, University of Cambridge, CB2 3EA, UK

[b]Image Analysis Group, Department of Applied Mathematics and Theoretical Physics (DAMTP), University of Cambridge, CB3 0WA, UK

[c] Department of Sustainable Agro-ecosystems and Bioresources, Research and Innovation Centre, Fondazione E. Mach, Via E. Mach 1, 38010 San Michele all'Adige (TN), Italy

[d] Environmental Change Institute, School of Geography and the Environment, University of Oxford, OX1 3QY, UK

[e] Centre for Biodiversity and Conservation Science, The University of Queensland, St Lucia, 4072, Qld, Australia

[f] Natural England, Cromwell House, 15 Andover Road, Winchester, SO23 7BT, UK

[g] Mullard Space Science Laboratory, University College London (UCL), Holmbury St Mary, Surrey RH5 6NT, UK

***Abstract*—Remote sensing of individual tree species has many applications in resource management, biodiversity assessment and conservation. Airborne remote sensing using LiDAR and hyperspectral sensors has been used extensively to extract biophysical traits of vegetation and to detect species. However, its application for individual tree mapping remains limited due to the technical challenges of precise co-alignment of images acquired from different sensors and accurately delineating individual tree crowns (ITCs). In this study we developed a generic workflow to map tree species at ITC-level from hyperspectral imagery and LiDAR data using a combination of well-established and recently developed techniques. The workflow uses a non-parametric image registration approach to co-align images, a multi-class normalised graph cut method for ITC delineation, robust principal component analysis for feature extraction, and support vector machine for species classification. This workflow allows us to automatically map tree species at both pixel- and ITC-level. Experimental tests of the technique were conducted using ground data collected from a fully-mapped temperate woodland in the UK. The overall accuracy of pixel-level classification was 91%, while that of ITC-level classification was 61%. The test results demonstrate the effectiveness of the approach, and in particular the use of robust PCA to prune the hyperspectral dataset and reveal subtle difference among species.**

***Index Terms*—Hyperspectral imaging, LiDAR, image registration, image segmentation, species classification, PCA, SVM, Wytham Woods**

I. Introduction

Having maps of individual tree locations is fundamental to understanding forest responses to global change, providing a basis for monitoring species distribution patterns, responses to stress, disease and exotic-species spread and deforestation [1]. Mapping species using conventional surveying methods requires a large amount of time and effort. Therefore, few tree maps extend beyond 50-ha (50 hectares). An example are larger scale maps that have been generated by sampling in small plots distributed over wider regions and interpolating them [2]. The development of sophisticated remote sensing technologies is making it increasingly feasible to monitor single trees in forests alternatively using satellites or aircraft. Satellite based multi-spectral sensors, such as WorldView-2, provide high resolution imagery covering visible and near infrared channels. These sensors are increasingly used for mapping species, but their effectiveness in species discrimination varies from study to study due to limited spectral resolution [3]–[6]. Airborne hyperspectral sensors, on the other hand, can measure spectral properties of a target in narrow bands ranging from visible to short-wave infrared wavelengths of the electromagnetic spectrum (400–2500nm). Studies carried out with handheld hyper-spectrometers show that species are often distinguishable from their leaf reflectance spectra, even in diverse tropical forests [7], [8]. For example, about half of 188 species sampled from a humid tropical forest in Hawaii could be distinguished from their spectra, with differential reflectance in the short wave infrared (SWIR) as well as the visible and new infrared (NIR) being important [8], [9]. Such results prognosticate the usability of remote sensing with similar sensors for identification of individual trees [10]–[13].

Airborne hyperspectral imaging provides spectral properties of the vegetation canopies, which can be used to identify tree species. Scaling-up species classification from leaf level to canopy level remains challenging as reflectance signals of mixed vegetation canopy are influenced by leaf density, leaf angle distribution, crown shape and shading [12]. Nevertheless, recent studies have successfully used hyperspectral imaging to map species in tropical forests [9], [14], [15], savanna woodlands [16], [17], Mediterranean woodlands [18], [19], temperate deciduous forests [20]–[22] and boreal forests [23], [24]. Clark *et al.* [14] pioneered the use of hyperspectral data to identify canopy species in tropical rain forest, detecting

seven tree species with 92% accuracy. Cho *et al.* [25] detected ten tree species with 57% accuracy in the lowveld woodlands of South Africa. Dalponte *et al.* [18] classified 23 species from two Mediterranean woodlands, and achieved 88% and 96% accuracy for those regions. Therefore, rapid advances are being made in this context.

The accuracy of pixel-level species maps can be improved by combining features from Light Detection And Ranging (LiDAR) and hyperspectral imagery in classification algorithms. LiDAR produces 3D point clouds indicating tree positions, from which canopy height and various other metrics can be extracted for each pixel. Features comprised of this structural information complement the optical data provided by hyperspectral sensors, particularly as LiDAR data is not influenced by illumination artifacts such as shading of shorter trees by their taller neighbours [26]. High species classification accuracy (89%) in an Italian temperate floodplain forest was achieved by fusing LiDAR and hyperspectral imagery before classification [26]. Jones *et al.* [27] showed that LiDAR and hyperspectral fusion can improve species classification in a mixed broadleaf-conifer forest. The work in [28] also showed that improvement was observed when LiDAR and hyperspectral imagery were used together in alpine forests containing a mixture of beech and conifers. However, the importance of LiDAR-derived features on classification success varies greatly among species [27]–[29].

The approaches described above illustrate the advances made in pixel-based classification, but less progress has been made in mapping individual tree crowns (ITCs) using multi-sensor techniques. The LiDAR 3D point cloud provides excellent data for ITC delineation [26]–[30], while canopy spectral information can be obtained from the corresponding pixels of hyperspectral imagery within each of the identified crowns, so in principle this combination of information is powerful [25], [31]–[35]. Mapping species at single tree scale has been demonstrated in urban environments, where trees are sparsely distributed [32]–[34], [36]. For example, Alonzo *et al.* [34] mapped 30 urban tree species at ITC-level using full spectral bands of hyperspectral imagery and seven tree structural parameters derived from LiDAR. However, for more complex environments, we know of only four studies that have investigated ITC-level species classification using a multi-sensor approach: Colgan *et al.* delineated ITCs from LiDAR and classified species from hyperspectral imagery in a savanna woodland, then combined these results [25]. Dinuls *et al.* [37] extracted tree tops from LiDAR, then classified five species from corresponding pixels taken from multi-spectral imagery. Heinzel and Koch showed that under-segmentation of ITCs using LiDAR-based delineation could be rectified by using species classification information alongside LiDAR [31]. Dalponte *et al.* improved species classification by only selecting pixels inside of ITCs in the training step of the classification [35]. Matsuki *et al.* [22] showed that LiDAR derived ITC features and shade correction of hyperspectral imagery could improve the accuracy of species classification. So this sort of analysis is still in its infancy.

This paper develops a generic workflow for tree species classification at ITC-level from LiDAR and hyperspectral sensors. We deal with several technical challenges:

- Multi-sensor imaging requires images recorded by various sensors need to be co-aligned. This is complicated by the fact that different sensor characteristics result in scale, rotation or translation mismatches between images, making correction a pre-requisite. Our workflow includes an image registration step using the NGF-Curv method [38] to co-align hyperspectral imagery and LiDAR.
- Locating ITCs in the 3D LiDAR point cloud or optical imagery requires an accurate tree delineation algorithm, but most established approaches are inaccurate in broadleaf forests [30], [39]. Our workflow includes a normalised graph cut scheme to delineate ITCs using LiDAR 3D point cloud information alongside optical imagery [40]. The effectiveness of our workflow will be demonstrated in a broadleaf forest.
- When selecting features for the classification, it is recognised that the dimensionality of hyperspectral data must be reduced to improve computationally efficiency. Moreover hyperspectral imagery may have a significant noise component, which make this selection challenging. We use robust PCA (rPCA) to prune the data, strip away some of the noise and select the most important features for the classification only [41].
- Finally, the tree species classification at both pixel-level and ITC-level is implemented using a support vector machine (SVM) [42].

The main contribution of this paper is the development of a systematic workflow to map tree species at both pixel-level and ITC-level from multi-sensor imagery utilizing a combination of new and established approaches, which provide a powerful new approach for tree mapping. We test the efficiency of this approach by working with airborne imagery collected over a 18-ha mapped stand of temperate woodland in the UK. Historically managed temperate forests are recognised as being particularly difficult for ITC delineation because they have relatively even upper canopies comprised of intercalated crowns. To the best of our knowledge, only four studies have explored ITC-level species classification in a temperate forest [4], [22], [31], [37].

The paper is organized as follows: in Section II, we introduce the temperate forest datasets tested in this paper. In Section III, we present our workflow for tree species classification at both pixel-level and ITC-level from LiDAR and hyperspectral sensors. The results and discussion are shown in Section IV. Conclusions and outlook are given in Section VI.

II. Data description

A. Study site and field data

Wytham Woods is a 385-ha deciduous forest, located in Oxfordshire, England (51°46′N, 1°20′W). A 18-ha forest plot was established in this wood in 2008 using standardised methods used in an international network of Smithsonian Institution Global Earth Observatories (SIGEO) [43]. Each hectare was delimited into 25 subplots of $20m \times 20m$. Every tree larger than 5cm diameter at chest height (DBH) was tagged, its DBH

measured, its species identified and its location mapped. There were 23 species of tree and shrub within the plot. In total, 20,308 stems and 16,313 individual trees were recorded (some trees had multiple stems). These plots were re-censused in 2009 and 2012, and the latest dataset was used in this study.

As subcanopy species and shrubs are hard to detect by remote sensing, this study focuses on mapping the six most dominant canopy tree species listed in Table I. Figure 1 shows the linkage between field data, and training and testing samples taken from the airborne survey. Tree height information is an important indicator for ITC-level species mapping. However, it was only measured on 389 individuals of these dominant canopy tree species. Species-specific functions were fitted to the height -diameters relationships ($H = a \ln DBH + b$, where a and b are coefficients estimated by linear regression) and these functions were used to estimate tree height information from DBH. We arbitrarily labeled trees >18m height as "canopy trees" (Table I) and used these to assess the accuracy of species detection.

TABLE I
THE NUMBERS OF INDIVIDUAL AND CANOPY TREES OF SIX SPECIES RECORDED IN WYTHAM PLOT

Species	Common name	No. of individual trees	No. of canopy trees
Fraxinus excelsior	European ash	5346	1249
Acer pseudoplatanus	Sycamore	7716	778
Larix decidua	European larch	99	98
Quercus robur	English oak	381	201
Fagus sylvatica	European beech	195	4
Betula spp.	Birch	85	16

B. Airborne survey

Airborne surveying was conducted in the Wytham Woods natural reserve on 24 June 2014 by the Airborne Research and Survey Facility of the UK Natural Environment Research Council (NERC-ARSF). The airplane flew at a nominal height above ground of approximate 800 m and was equipped with LiDAR and hyperspectral imagers. LiDAR and hyperspectral imagery were pre-processed by NERC-ARSF Data Analysis Node.

Hyperspectral imagery was obtained by the AISA Fenix sensor, which is a pushbroom imaging array sensor with 384 cross-track pixels and provides 361 spectral bands from visible to shortwave infrared (0.4–2.5μm) region. The field of view of the AISA Fenix sensor is 31.94°. In this study, a single flight line of hyperspectral imagery was used, so illumination and sensor geometry was similar for all pixels. Atmospheric correction was not applied to the hyperspectral imagery. Although adjacency effects can influence the classification accuracy and atmospheric correction can reduce this problem, a number of studies have reported that applying an atmospheric correction has little effect on species classification [26], [35], [44], [45]. A bi-directional distribution function (BRDF) correction was not applied since a single flight line was used. If the hyperspectral imagery had been obtained from several flight lines, radiometric normalisation would have been needed in our workflow (Figure 2). The hyperspectral imagery was orthorectified and georeferenced in Ordinary Survey Great Britain (OSGB) projection, with spatial resolution of 1.2 m. The airborne LiDAR data were acquired by Leica ALS-50 II sensor. A scan angle of 12° was used. The LiDAR data were originally captured in full wave-form, however, they were converted to discrete LiDAR point cloud during the pre-processing step, within which the LiDAR point cloud was georeferenced in OSGB projection. The final point density was approximately 6 points/m^2. The equipment on board the NERC aircraft is regularly calibrated to ensure that LiDAR data are accurately georeferenced and the hyperspectral imagery is radiometrically calibrated before delivery.

III. METHOD

In this section, we present our processing workflow for pixel-level and ITC-level tree species classification from LiDAR and hyperspectral imagery, see Figure 2. The co-alignment step uses the NGF-Curv image registration method [38], the feature extraction from hyperspectral imagery is carried out with the rPCA method [41], the ITC delineation step uses a LiDAR point cloud based clustering method that is informed by hyperspectral information called MC–RC [40], and, finally, the tree species classification at pixel-level and ITC-level is conducted with a SVM classifier [42] with the majority voting rule over each delineated crown area. The workflow in Figure 2 is very general, and the methods are described in greater detail below.

A. Co-alignment of LiDAR and hyperspectral imagery

Co-alignment of LiDAR and hyperspectral imagery can be achieved by ground control points or by unsupervised image registration. Our NGF-Curv method adopts the latter approach [38]. The true colour composites of Red, Green and Blue (RGB) bands (640, 549 and 460 nm) of hyperspectral imagery were converted to greyscale images by MATLAB's built-in function `rgb2gray` and the greyscale image was used for the registration. LiDAR was converted to a digital surface model (DSM) – interpolating LiDAR first returns. The DSM was used for the registration. Let reference (R) and template (T) images be the DSM taken from LiDAR and the greyscale image obtained from the hyperspectral imagery, respectively. The LiDAR DSM image was used as the reference image because the spatial resolution of the LiDAR DSM image was more accurate than that of the hyperspectral imagery. Reference R and template T are modelled as functions defined on a finite 2D grid Ω, mapping a point x on the grid to a real intensity value $R(x)$ and $T(x)$, respectively. The objective of the image registration is to find an optimal transformation mapping $u : \Omega \to \Omega$ that co-aligns the template image to the reference image. The NGF-Curv method we used computes the transformation u as a minimizer of an energy that consists of a similarity term D and a regularisation term S. That is, u is the solution of the following problem

$$\min_u \Big\{ \sum D[R(x), T(u(x))] + \alpha S(u) \Big\}$$

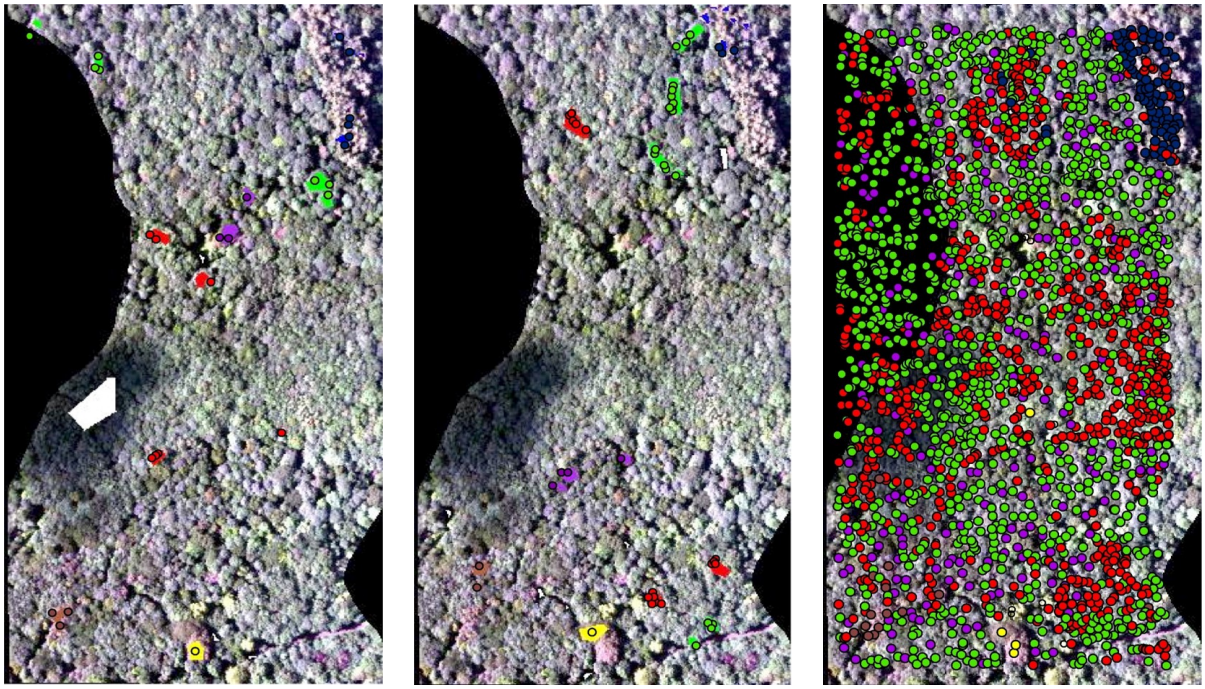

(a) Training samples (b) Test samples (c) Ground truth

Fig. 1. Training and testing samples for species classification in Wytham Woods. The coloured points in panel (a), (b) and (c) are ground truth overlaid over a false colour representation of the hyperspectral imagery. The coloured polygons in (a) and (b) represent training and testing samples of each species overlaid over a false colour representation of the hyperspectral imagery. Colours indicate different species, i.e., blue = *Larix decidua*, green = *Acer pseudoplatanus*, red = *Fraxinus excelsior*, yellow = *Fagus sylvatica*, purple = *Quercus robur*, brown = *Betula* spp., and white = shaded pixels.

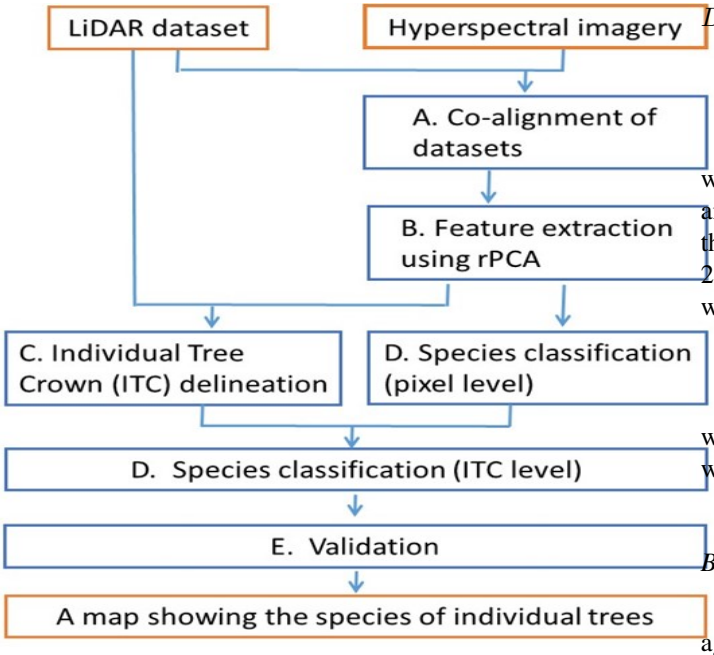

Fig. 2. Workflow used to detect individual tree crown and identify their species by fusing LiDAR and hyperspectral imagery.

where α is the regularisation parameter which balances the similarity term and the regularisation term. The similarity term D used is defined by

$$1 - \left[\left(\frac{\nabla T(u)}{\sqrt{|\nabla T(u)|^2 + \eta^2}} \right)^t \left(\frac{\nabla R}{\sqrt{|\nabla R|^2 + \eta^2}} \right) \right]^2,$$

which is the so called NGF distance measure, where $\eta > 0$ is an edge parameter which represents the level of the noise in the images and ∇^t is the transpose of the discrete gradient in 2D. To impose smoothness features on the transformation u we use the curvature in the regularisation term S, i.e.

$$S(u) = \frac{1}{2} \sum_{x \in \Omega} |\Delta u(x)|^2,$$

where Δ is the discretised Laplace operator. For more details, we refer to [38] and references therein.

B. Feature extraction

Extracting feature information from the hyperspectral imagery is a key step to map individual trees with species information. As the hyperspectral imagery contains 361 spectral bands (i.e. dimensionality is high), the meaningful features are hidden inside an enormous number of spectral bands. To extract the most meaningful features, a data pruning technique rPCA [41] is implemented in our workflow.

Let M be a $m \times n$ measurement matrix, where m is the number of spatial pixels of the hyperspectral imagery, n is the number of spectral bands of the hyperspectral imagery. Principal component analysis (PCA) finds a rank k matrix L

from M, which may be corrupted by noise. It can be expressed by the following minimisation problem:

$$\min_{L}\{\|M-L\|_2\} \quad \text{s.t.} \quad \mathcal{R}(L)<k, \tag{1}$$

where $\|\cdot\|_2$ is the ℓ_2-norm, and $\mathcal{R}(\cdot)$ is the operator computing the rank of the given matrix. Problem (1) is solved explicitly by singular value decomposition. However, the PCA is sensitive to the magnitude of noise in the data [46], thus it may not be suitable for extracting meaningful features from hyperspectral data. The rPCA method has been proposed to improve the robustness of the PCA method [41]. It aims to recover a low rank matrix L from the noisy measurement matrix M, which is the hyperspectral imagery in our case, by removing a sparse outlier matrix S. The rPCA method can be represented by the following minimization problem:

$$\min_{L,S}\{\mathcal{R}(L)+\lambda\|S\|_0\} \quad \text{s.t.} \quad M=L+S, \tag{2}$$

where $\|\cdot\|_0$ is the ℓ_0-norm which counts the number of the nonzero entries therefore imposing sparsity property on S, and λ is a regularisation parameter which balances the importance between the ranking operator and the sparsity regularisation. This is a non-convex optimisation problem whose solution is in general NP-hard. To make the optimisation problem (2) tractable, its convex relaxation using the nuclear norm $\|\cdot\|_*$ (sum of singular values) and the l_1-norm (sum of the absolute values of all entries) were adopted instead of $\mathcal{R}(\cdot)$ and the l_0-norm respectively. This results in the following convex problem:

$$\min_{L,S}\{\|L\|_*+\lambda\|S\|_1\} \quad \text{s.t.} \quad M=L+S. \tag{3}$$

More details about rPCA can be found in [41] and references therein. Since (3) is a convex problem, it can be solved effectively by, for example, the alternating direction method for multipliers (ADMM) [47]. In fact, the parameter λ is fixed to $\frac{1}{\sqrt{m}}$. The validity of the parameter choice of λ is given by [41, Theorem 1]. Robust PCA reduces the dimensionality of the hyperspectral imagery in a robust way. In addition, a user can prune the data further. The performance of rPCA will be discussed in section V.

C. Individual tree crown delineation

Individual tree crown delineation is performed by a normalised graphcut method constrained by prior knowledge directly on the 3D LiDAR point clouds and the extracted features from subsection III-B. See [48] and method MC–RC in [40] for a detailed explanation of the methodology.

Let $\boldsymbol{G}$ be a graph containing a set of pairs, $\boldsymbol{G}=(\boldsymbol{\nu},\boldsymbol{\epsilon})$, where $\boldsymbol{\nu}$ is the set of vertices and $\boldsymbol{\epsilon}$ is the set of edges. Each edge $w(\nu_i,\nu_j)\in\boldsymbol{\epsilon}$ corresponds to the non-negative similarity weight w_{ij} between two vertices ν_i and ν_j. Such a graph is built using the LiDAR point clouds. The similarity weights depend on Euclidean distances between the LiDAR points as well as extracted features from hyperspectral imagery. The details of how to define the weights is given by [40].

Let $\boldsymbol{W}$ be an $N\times N$ symmetric matrix with entries $\boldsymbol{W}(i,j)=w_{ij}$ given by the weights, $\boldsymbol{D}$ be an $N\times N$ diagonal matrix with diagonal entries $d_i=\sum_j w_{ij}$, $\mathbf{1}$ be an $N\times 1$ all-ones vector, $\boldsymbol{I}$ be a $C\times C$ identity matrix and $\boldsymbol{X}$ is the unknown labelling, which is an $N\times C$ matrix, where C is the number of clusters in the point cloud. The normalised cut seeks an optimal labelling $\boldsymbol{X}$ as the solution of

$$\begin{aligned}&\min_{\boldsymbol{X}}\operatorname{tr}\big(\boldsymbol{X}^T\boldsymbol{D}^{-\frac{1}{2}}(\boldsymbol{D}-\boldsymbol{W})\boldsymbol{D}^{-\frac{1}{2}}\boldsymbol{X}\big)\\ &\text{s.t.}\quad \boldsymbol{X}^T\boldsymbol{D}^{\frac{1}{2}}\mathbf{1}=\mathbf{0},\quad \boldsymbol{X}^T\boldsymbol{X}=\boldsymbol{I},\end{aligned}$$

where $\operatorname{tr}(\cdot)$ is the trace of a matrix.

In our algorithm the original normalised cut is relaxed as a convex optimisation problem, and guided by prior information about the likely location of trees. It is not straightforward to incorporate prior knowledge in normalised graphcut, as the normalised cut finds optimal partitioning from the graph of the similarity weights. In our modified scheme, prior information is regarded as an additional constraint in the normalised graphcut approach. It minimises the normalised cut energy as well as satisfying a correlation constraint with priors. The correlation term $\operatorname{diag}(\boldsymbol{X}^T\boldsymbol{S})=\kappa\operatorname{diag}(\boldsymbol{I})$ incorporates a prior information matrix $\boldsymbol{S}$, which consists of the local maxima of the canopy height model (CHM) and their neighbour points. Here κ is a correlation coefficient. The CHM was obtained by subtracting bare-earth topography from the DSM. Our modified multiclass normalised graphcut can be written as:

$$\begin{aligned}&\min_{\boldsymbol{X}}\operatorname{tr}\big(\boldsymbol{X}^T\boldsymbol{D}^{-\frac{1}{2}}(\boldsymbol{D}-\boldsymbol{W})\boldsymbol{D}^{-\frac{1}{2}}\boldsymbol{X}\big)\\ &\text{s.t.}\quad \operatorname{diag}(\boldsymbol{X}^T\boldsymbol{X})=\operatorname{diag}(\boldsymbol{I}),\quad \boldsymbol{X}^T\boldsymbol{D}^{\frac{1}{2}}\mathbf{1}=\mathbf{0},\\ &\qquad\quad \operatorname{diag}(\boldsymbol{X}^T\boldsymbol{S})=\kappa\operatorname{diag}(\boldsymbol{I}).\end{aligned}$$

The locations of local maxima were computed by the toolbox for LiDAR data filtering and a standard forest analysis (TIFFS, Globalidar ltd.) [30]. Although we used TIFFS for extracting priors, users could use any tree top searching algorithm to get priors. We refer to [40] for more details.

D. Species classification

For the classification of the tree species we used the SVM method, that is a non-parametric supervised classifier, which has been showed to be superior to other classification strategies in several studies [23], [26], [35], [49], [50]. We applied SVM on the extracted features from subsection III-B in order to classify species, initially at the pixel level.

For a training data set $\mathcal{T}=\{(x_1,y_1),\cdots,(x_n,y_n)\}$ consisting of pairs of feature vectors $x_i\in\mathcal{F}$ (where $\mathcal{F}\subset\mathbb{R}^m$ is a m-dimensional feature space), and labels y_i (for example the binary label $y_i\in\{-1,1\}$ in the case of two species). Then, SVM finds a separating hyperplane $H:=\{x\mid\langle w,\eta(x_i)\rangle-b=0\}$ (where w is a normal vector to the hyperplane, b is the intercept and $\eta(x_i):\mathcal{F}\to\bar{\mathcal{F}}$ is a non-linear embedding that transforms the original feature space to a higher dimensional space). H has dimension depending on the number of species (labels) in y_i although typically the dimension is 1 (SVM for binary classification). In this study, we adopt the radial basis (RBF) kernel $\exp(-\gamma\|x-x'\|_2^2)$ for η, where γ is the parameter for the radial basis. Therefore, the higher dimensional space $\bar{\mathcal{F}}$ is where the radial basis functions lives.

The hyperplane H is then obtained by minimising the following model

$$\begin{aligned} &\min_{w,b,\xi} \|w\|_2^2 + C\sum_{i=1}^{n}\xi_i \\ &\text{s.t.} \quad y_i \cdot (\langle w, \eta(x_i)\rangle - b) \geq 1 - \xi_i \\ &\qquad \xi_i \geq 0 \end{aligned}$$

where C is a regularisation parameter and $\xi_i = \max(0, 1 - y_i \cdot \langle w, \eta(x_i)\rangle - b)$ is called a slack variable, which takes into account non-separable data.

SVM is an intrinsically binary classifier, but it can be extended to multi-class problems by following two different strategies: one-against-one and one-against-all. In this study, we use the one-against-all rule, which solves K binary problems instead of solving a K-class problem. We refer to [42] and references therein for an excellent introduction to SVM. A Library for SVM (libSVM) for MATLAB was used to solve the multi-class SVM problem [42]. The optimal parameters for SVM classification were found by trial and error. The regularisation parameter C was fixed to 100, and the parameter γ was set to 0.5 for all experiments in Section IV.

Figure 3 (a) and (b) show the location of the training and test samples used for the pixel-level tree species classification evaluation. Table II shows the number of pixels for each species used as training and test samples. The training and test samples of the hyperspectral imagery were extracted from manually delineated ITC by means of visual inspection and field data. We considered only trees with height above 18m. It makes sense to mask out understory trees since spectral signatures captured from the hyperspectral imagery mainly originate from canopy leaves. The ITC-level tree species classification map is obtained by extracting the pixel level map for each ITC and applying a majority voting rule [9], [35] to decide the species for each crown (ITC-level). Therefore, the most frequent species class inside of each ITC represents the species of ITCs.

E. Validation

The tree species classification was evaluated at both pixel- and ITC-level. The confusion matrix and reliability scores were used to evaluate the accuracy of species classification. Producer's, user's and overall accuracies were computed starting from the confusion matrix. In addition, cohen's kappa, quantity and allocation disagreement were computed for the reliability of the classification results (see Table III, IV and V) [51].

IV. Results

This section presents the experimental results of our individual tree species classification approach. We present the results of using both PCA and rPCA in the feature extraction step of the workflow to explore whether rPCA delivers more accurate results over the traditional approach. We refer to workflows using PCA and rPCA in the feature extraction step as the ITSC and ITSC-R methods, respectively. For the results shown here, the feature extraction was applied only to the hyperspectral imagery.

Figure 4 summarises the results of steps A, B and C of the workflow: Figure 4 (a) and (b) show the LiDAR (CHM) and a false colour representation of the hyperspectral imagery, and Figure 4 (c) shows the co-alignment result using the NGF-Curv registration method [38]. Since the initial alignment between LiDAR and hyperspectral imagery was excellent, any errors were too small to be apparent visually in our dataset. Figure 4 (d)–(g) show the first three principal components obtained by the rPCA method and their RGB colour composite. In our workflow, the first 20 principal components were used to delineate ITCs along with LiDAR using the MC–RC [40], and classify species at the pixel and ITC levels. Figure 4 (h)–(j) show the ITC delineation results.

A. Pixel-level tree species classification

Figure 3 (c) shows the species classification results over the 18-ha field plot in Wytham Woods. The results for the test samples, presented in Tables III and IV, show the overall accuracy of the ITSC-R method at pixel-level was 91.7% while that of the ITSC method was 85.8%. In overall, the ITSC-R method performed better than the ITSC method.

Regarding the individual species, for *Fraxinus excelsior* , the producer's accuracy was 92.0 % for both ITSC-R and ITSC methods, but the ITSC-R method performed better with respect to the user's accuracy. The ITSC-R method outperformed the ITSC method for producer's accuracy and user's accuracy of *Acer pseudoplatanus*. The ITSC-R method showed better performance with respect to producer's accuracy for *Quercus robur*, while user's accuracies were poor for both ITSC-R and ITSC methods. The confusion matrices of both ITSC-R and ITSC methods (Tables IV and III) show that *Fraxinus excelsior* was confused mainly with *Acer pseudoplatanus* and *Quercus robur*. *Acer pseudoplatanus* was confused with *Fraxinus excelsior* and *Quercus robur*. This is the reason for the low user's accuracy of *Quercus robur*. It makes sense as the ground truth data in Figure 5 clearly shows that these three species are dominant in the study site and often are mixed. *Larix decidua* was dominant at the north east edge of the study site, and both ITSC-R and ITSC methods successfully classified all the test samples of this species. However, *Larix decidua* was one of the major confusing factor for *Fagus sylvatica* pixels, so the user's accuracy of *Larix decidua* was poor for the ITSC method. The producer's accuracy of *Fagus sylvatica* was only 70.0% for the ITSC method as it was confused with *Quercus robur* and *Larix decidua* pixels. For the ITSC-R method, the producer's and user's accuracies of *Fagus sylvatica* were 91.0% and 94.3%, respectively. The producer's accuracy of *Betula* species were only 61.2% for the ITSC method, while the ITSC-R method achieved 74.2% producer's accuracy. With respect to the user's accuracy of *Betula* species, the ITSC-R method achieved 98.6%, while the ITSC method only had 83.8%.

B. ITC-level species classification - mapping individual trees

Species classification at ITC-level was validated using software specifically designed for validating tree segmentation,

!h

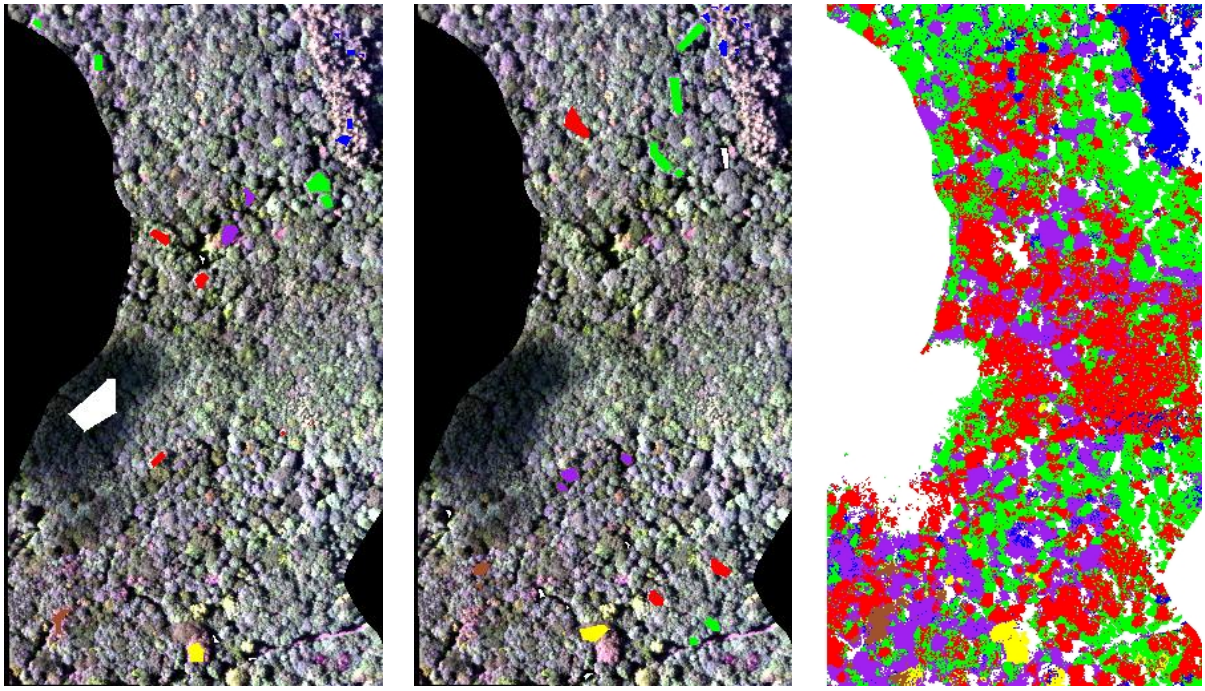

(a) Training samples (b) Test samples (c) Species classification map

Fig. 3. The pixel-level species classification in Wytham Woods. The coloured polygons in (a) and (b) represent training and test samples of each species overlaid over a false colour representation of the hyperspectral imagery. The colour map (c) shows the result of the pixel-level species classification by our proposed workflow. Colours indicate different species, i.e., blue = *Larix decidua*, green = *Acer pseudoplatanus*, red = *Fraxinus excelsior*, yellow = *Fagus sylvatica*, purple = *Quercus robur*, brown = *Betula* spp., and white = shaded pixels

TABLE II
NUMBER OF PIXELS FOR EACH SPECIES OF THE TRAINING AND TEST SAMPLES FOR TREE SPECIES CLASSIFICATION

Species	Training samples	Test samples
Fraxinus excelsior	226	410
Acer pseudoplatanus	304	431
Larix decidua	126	129
Quercus robur	178	149
Fagus sylvatica	139	199
Betula spp.	93	93
Shade	844	126
Overall (NO. of pixels)	1910	1537

called the NewFor software. [52], [53]. This software uses tree heights and tree locations to find the best matching candidates between the ground truth and the segmented tree crowns. The software, therefore, is sensitive to the initial positioning of the ground truth. To alleviate this problem, we also included two figures to evaluate species classification at ITC-level. Figure 5 shows the both pixel- and ITC-level species classification results along with the ground truth information. Figure 6 shows the map of ITCs of each species using MC–RC method and the ground truth data. These two figures will be used to compare the patterns of species distribution across the study site.

In total, 1687 ITCs were delineated by MC–RC algorithm. However, the NEWFOR algorithm used to test delineation accuracy indicated that 683 ITCs were correctly delineated. The number of false positives generated by our algorithm were 1004, while 1002 ground truth trees were missing. The performance of ITC-level species classification was examined only for the 683 ITCs, which were corrected delineated by the validation software. However, the visual analysis of Figure 6 showed that the validation software does not accurately describe the performance of the ITC-level species classification. For example, *Larix decidua* is dominant at the north east edge of the study site. Since *Larix decidua* is a coniferous tree, it is relatively easy to delineate its crowns accurately. However, the validation results and table V show that almost 87% *Larix decidua* trees were omitted according to the validation results.

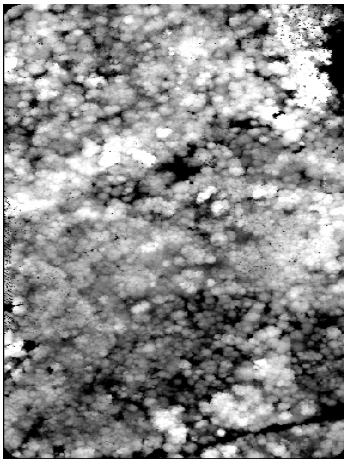

(a) LiDAR

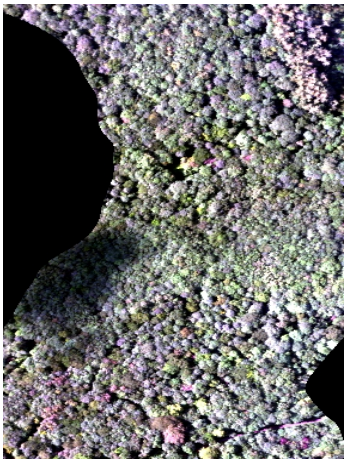

(b) Hyperspectral imagery

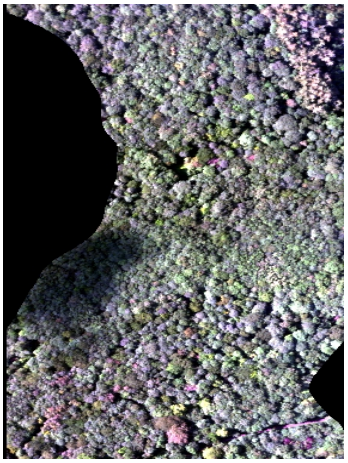

(c) Co-aligned hyperspectral imagery

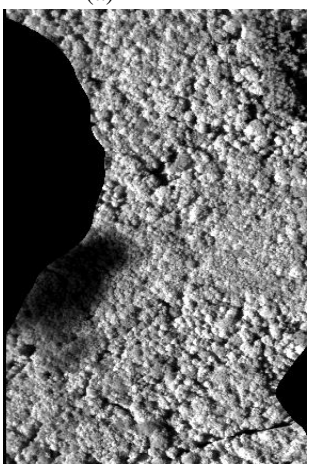

(d) 1^{st} principal component

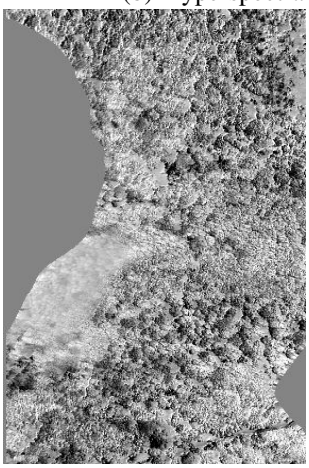

(e) 2^{ed} principal component

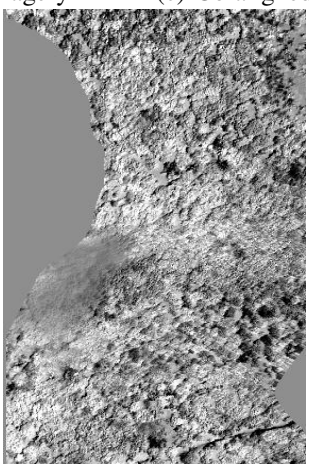

(f) 3^{rd} principal component

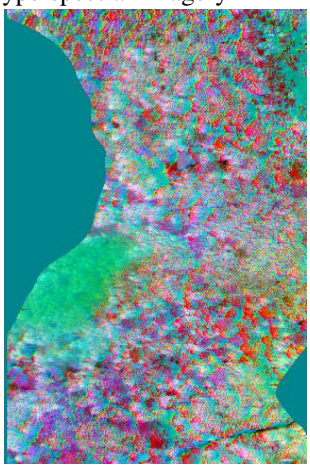

(g) Colour composite of the first 3 principal components

(h) ITCs of *Fraxinus excelsior*

(i) ITCs of *Acer pseudoplatanus*

(j) ITCs of *Quercus robur*

Fig. 4. The results of the images co-alignment, feature reduction and ITC delineation in our workflow. The first row shows the image registration between LiDAR DSM (a) and RGB true colour hyperspectral imagery (b) and the co-aligned hyperspectral imagery in RGB true colour (c). The second row shows the first three principal components (d)-(g). The third row shows examples of the MC–RC segmentation viewed obliquely (h)-(j) and different colours represent ITCs.

In Figure 6(d) and (j), the patterns of *Larix decidua* from segmented ITCs and ground truth field data were very similar. This is mainly because the software is sensitive to the accuracy of tree coordinates in the ground data. Horizontal and vertical distances within 5 m between ground and segmented trees are considered to be matched. Since ground truth dataset had positioning errors of around 10 metres, large commission and omission errors arose.

TABLE III
SPECIES CLASSIFICATION RESULTS OBTAINED BY THE ITSC METHOD, BASED ON PCA

		Ground truth								
	Species	*Fraxinus excelsior*	*Acer pseudoplatanus*	*Larix decidua*	*Quercus robur*	*Fagus sylvatica*	*Betula* spp.	Shade	Total	Producer's accuracy (%)
Classification results	*Fraxinus excelsior*	377	24	1	7	0	0	1	410	92.0
	Acer pseudoplatanus	48	356	3	24	0	0	0	431	82.6
	Larix decidua	0	2	125	0	0	2	0	129	96.9
	Quercus robur	0	0	5	143	0	1	0	149	96.0
	Fagus sylvatica	0	7	18	25	139	8	2	199	70.0
	Betula spp.	3	6	1	22	4	57	0	93	61.2
	Shade	0	0	0	4	0	0	122	126	96.8
	Total	428	395	153	225	143	68	125	1537	
	User's accuracy (%)	88.1	90.1	81.7	63.6	97.2	83.8	97.6		85.8

Kappa accuracy = 0.825, Quantity disagreement = 0.077, Allocation disagreement= 0.065

TABLE IV
SPECIES CLASSIFICATION RESULTS OBTAINED BY THE ITSC-R METHOD, BASED ON RPCA

		Ground truth								
	Species	*Fraxinus excelsior*	*Acer pseudoplatanus*	*Larix decidua*	*Quercus robur*	*Fagus sylvatica*	*Betula* spp.	Shade	Total	Producer's accuracy (%)
Classification results	*Fraxinus excelsior*	377	16	0	13	0	0	4	410	92.0
	Acer pseudoplatanus	11	390	2	28	0	0	1	431	90.5
	Larix decidua	0	0	129	0	0	0	0	129	100
	Quercus robur	0	0	0	148	1	0	0	149	99.3
	Fagus sylvatica	0	0	3	10	181	1	4	199	91.0
	Betula spp.	0	1	12	1	10	69	0	93	74.2
	Shade	0	0	8	2	0	0	116	126	92.1
	Total	388	407	137	219	192	70	124	1537	
	User's accuracy (%)	97.2	95.8	94.1	67.6	94.3	98.6	93.6		91.7

Kappa accuracy = 0.898, Quantity disagreement = 0.051, Allocation disagreement= 0.032

TABLE V
SPECIES CLASSIFICATION RESULTS AT ITC-LEVEL.

		Ground truth								
	Species	*Fraxinus excelsior*	*Acer pseudoplatanus*	*Larix decidua*	*Quercus robur*	*Fagus sylvatica*	*Betula* spp.	Other species	Total	Producer's accuracy (%)
Classification results	*Fraxinus excelsior*	146	38	4	36	0	0	0	224	65.2
	Acer pseudoplatanus	82	205	3	50	0	1	0	341	60.2
	Larix decidua	5	2	4	2	0	0	0	13	30.8
	Quercus robur	4	19	0	53	0	1	0	77	68.8
	Fagus sylvatica	1	0	0	0	3	0	0	4	75.0
	Betula spp.	2	0	0	1	0	6	0	9	66.7
	Other species	9	5	1	0	0	0	0	15	0
	Total	249	269	11	143	3	8	0	677	-
	User's accuracy (%)	58.6	76.2	37.1	36.4	100	75.0	0	-	61.1

Kappa accuracy = 0.410, Quantity disagreement = 0.133, Allocation disagreement= 0.256

Table V shows the confusion matrix at ITC-level, which considers only correctly assigned ITCs. The overall accuracy was only 61.1%, which was lower than that at pixel level. *Fraxinus excelsior* classification indicates that both producer's and user's accuracies were poor, while visual comparison of ground truth and species map in Figure 5 and Figure 6(a) and (g) show that species distribution patterns of ground truth and species map had a good agreement. The ITC-level classification of *Acer pseudoplatanus* was 65.2% and 58.6% with respect to producer's and user's accuracies. Visual inspection of Figure (b) and (h) suggested that ITC-level mapping of *Acer pseudoplatanus* agreed well with the ground truth data. *Larix decidua* was excluded from the validation as the ITC-level detection was unrealistic, but visual comparison implies that species distribution of pixel- and ITC-level were well agreed with the ground truth data. *Quercus robur* had a good producer's accuracy, while its user's accuracy was only 36.1%. This was in accordance with the pixel-level classification of *Quercus robur*. In particular, visual analysis of the ITC delineation suggests that *Quercus robur* was oversegmented (see Figure 6 (c) and (i). This might be because some branches were extracted as different local maxima, so the segmentation algorithm oversegmented the oak trees. The accuracy of *Fagus sylvatica* had high producer's accuracy and user's accuracy.

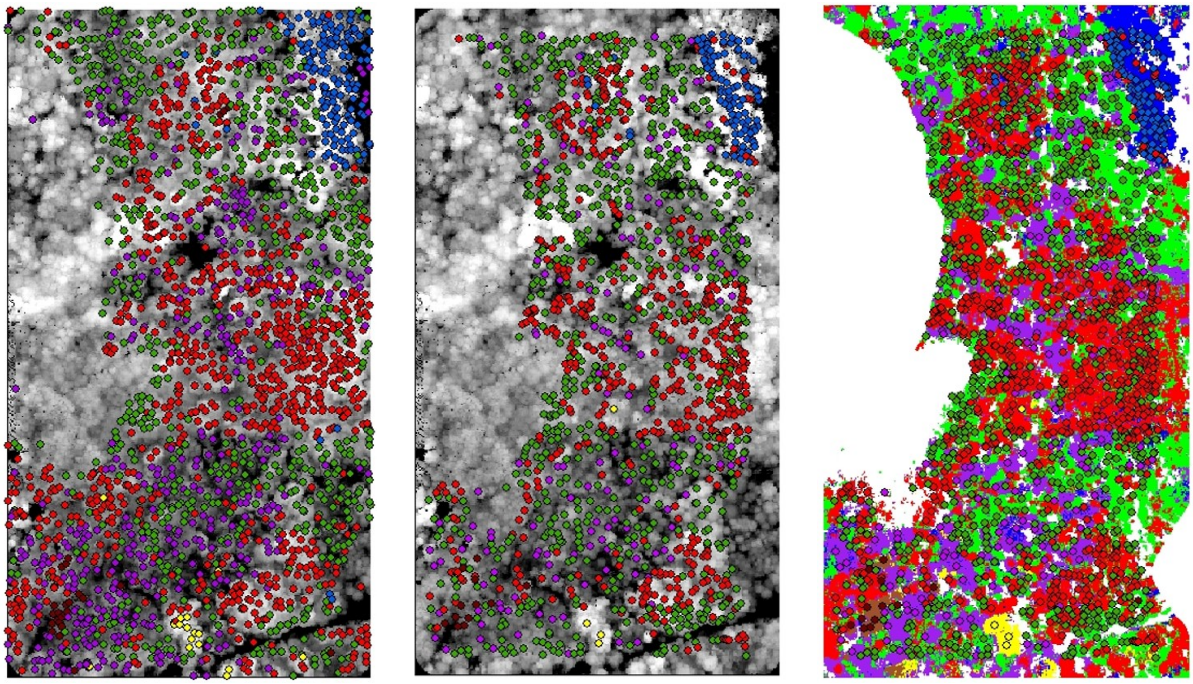

(a) ITC species mapping (b) Ground truth (c) Ground truth with pixel-level species classification

Fig. 5. Mapping individual tree species at ITC-level and ground truth. The background images in (a)-(c) are DSM. The coloured map in (c) is pixel-level species classification, where each colour indicates different species. The circles in colours represents ITCs of different species. blue = *Larix decidua*, green = *Acer pseudoplatanus*, red = *Fraxinus excelsior*, yellow = *Fagus sylvatica*, purple = *Quercus robur*, brown = *Betula* spp.

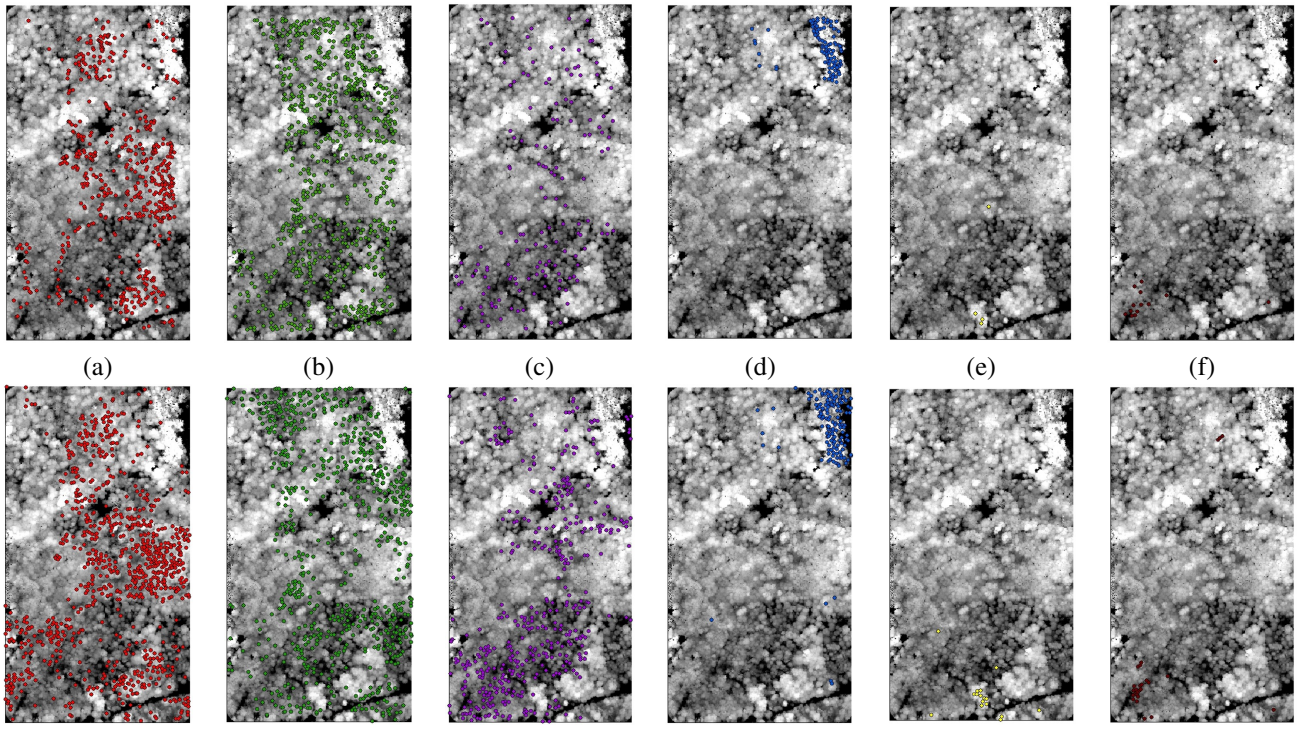

(a) (b) (c) (d) (e) (f)

(g) (h) (i) (j) (k) (l)

Fig. 6. Mapping each species at ITC-level and the ground truth. Each circle represents a single ITC. The first row shows the ground truths canopy trees over 18m. The second row shows the results of ITC-level species classification. Colours indicate different species, i.e., blue = *Larix decidua*, green = *Acer pseudoplatanus*, red = *Fraxinus excelsior*, yellow = *Fagus sylvatica*, purple = *Quercus robur*, brown = *Betula* spp.

Oversegmentation was observed in visual inspection. This was partly because we only selected canopy trees over 18m, so some canopy trees were omitted. In addition, some branches of *Fagus sylvatica* were identified as local maxima, thereby causing commission errors. The accuracy of *Betula* spp. was relatively high compared to other species. *Betula* spp. are located in a small area at southwest edge of the study site, so they can be mapped more easily (Figure 6 (f) and (l)).

V. Discussion

The rPCA feature reduction technique provides a rich information for distinguishing species with far fewer dimensions than the original hyperspectral datasets. Figure 7 (a) shows that spectral radiance of *Fraxinus excelsior* and *Acer pseudoplatanus* are similar to each other and have greater radiance values than other species. The first few principal components of PCA and rPCA reveal the same pattern, with *Fraxinus excelsior* and *Acer pseudoplatanus* having higher coefficients than the other species (Figure 7 (b) and (c)). It is important to note that PCA coefficients of different species tend to be similar for higher axes, so have little value in guiding species classification. In contrast, the coefficients from higher rPCA bands are very different among species, so provide meaningful signals with which to identify species. How to select the best number of principal component feature to give in input to the classifier is another challenging question. In our case, rPCA reduced the dimensionality of the data from 361 to 32. After visually examining the noise in each PC axis, we selected the first 20 PCs. The sensitivity analysis of the pixel-level classification accuracy with respect to different numbers of PC feature inputs is presented in Figure 8. In overall, the pixel-level classification using rPCA showed at least the same or better accuracy. The best pixel-level classification accuracy using rPCA was achieved when we considered the first 22 PCs (92.19%). Then it decreased slightly. On the other hand, PCA achieved the best classification accuracy with the first 43 PCs (91.41%).

In this study, pixel-level species classification was conducted using only hyperspectral imagery, because our emphasis was on improving species classification from hyperspectral imagery using rPCA technique. Many studies have reported that using LiDAR features can improve species classification, since LiDAR is not influenced by illumination artefacts [23], [26]–[28]. LiDAR intensity may provide more detailed radiometric information for guiding species classification, however, in our acquisition LiDAR intensity was controlled in non-linear way by automatic gain control, thus it was not possible to calibrate the intensity and to use it for species classification. In addition, illumination information is important for finding shaded pixels in our method, so the improvement by additional features from LiDAR may not be significant. Investigating the role of LiDAR derived metrics on species classification could provide better understanding of species classification [22], but this is the beyond of the scope of this paper.

Species classification at pixel level is strongly influenced by illumination effects [14], [31], [35], [54]. Species classification using only sunlit pixels produce better results than considering all pixels [14]. Thus a shadow removal step may be seen as a pre-requisite. Shadow removal can be done by manual selection [14], [29], ray tracing simulation with LiDAR derived DSM [54], ITC information from LiDAR [31] or normalised difference vegetation index filtering [34]. In this study, shaded pixels were included as additional class for learning (see Figure 3), such that shaded pixels were detected during the pixel-level species classification process as previously suggested by [26]. This strategy is particularly useful as we can detect shaded pixels without particularly processing the shaded area. The producer's and user's accuracies of shaded pixel detection were high in both ITSC and ITSC-R methods. It is well-known that the first principal component is mainly related with illumination effects [55], which may be linked with high accuracy of shaded pixel detection of our method. Although Tochon *et al.* [55] report that the first component of PCA is not useful for ITC delineation, it can, at least, be used for more accurate pixel-level species classification by detecting shaded pixels.

The size of training dataset may affect the species classification result. In this paper Approximately 1–7 crowns per species were used to classify all species and shaded pixels. Baldeck and Asner [56] showed that the sensitivity of species classification on sample size is dependent on the number of species and spectral separability of each species. In that study, the optimal number of tree crowns for species classification in a savanna woodland was 10 trees for two species and 19 trees for eleven species; i.e. they used more tree samples. This difference might be related with the types of forest. We tested our workflow in a temperate forest, while their research was conducted in a savanna woodland. We also used robust PCA to reduce 361 spectral bands to 20 principal components, so direct comparison of these papers may not work. Moreover, airborne hyperspectral imagery used in this paper contained spectral signals spanning from the visible to SWIR (400–2500nm) wavelength region, while, the spectrometer used by [56] had spectral coverage from visible and NIR wavelength region (400–1000nm). The SWIR region may give more spectral separability, so it could reduce the sample size needed for species classification. Finding an optimal size of training samples in our test site requires further analysis, but we leave it for future work.

VI. Conclusion and outlook

This study investigated the possibility of species mapping using airborne remote sensing datasets. Although several algorithms have been suggested for species mapping over various types of forest, their system architectures assumed co-alignment of LiDAR and hyperspectral imagery, so it was difficult to apply directly. In addition, their methodologies for delineating ITC were mostly based on digital surface models rather than LiDAR point cloud, so both forest and ITC parameter estimation were relatively inaccurate. We introduced 3D tree delineation algorithm MC–RC in our workflow, so forest analysis at species level, such as total biomass estimation of each canopy species, can be conducted more accurately. Our workflow has provided a general framework to fuse multi-sensor imagery and demonstrated its efficiency in a mixed

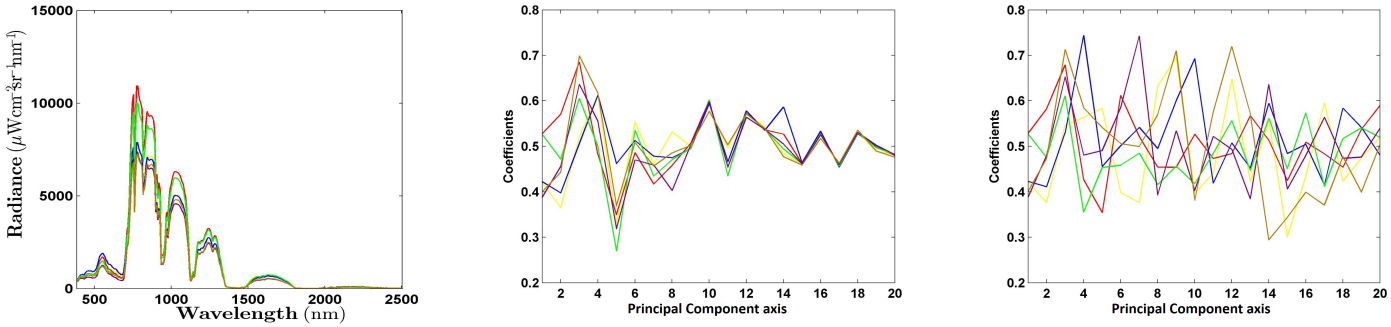

(a) Mean spectra (b) PCA coefficients (c) rPCA coefficients

Fig. 7. Spectral signatures and principal component coefficients of six dominant canopy tree species. Panel (a) shows spectral signatures of species, (b) and (c) are the mean coefficients of PCA and rPCA of species, respectively. Colours in (a)–(c) represent different species, i.e., blue = *Larix decidua*, green = *Acer pseudoplatanus*, red = *Fraxinus excelsior*, yellow = *Fagus sylvatica*, purple = *Quercus robur*, brown = *Betula* spp.

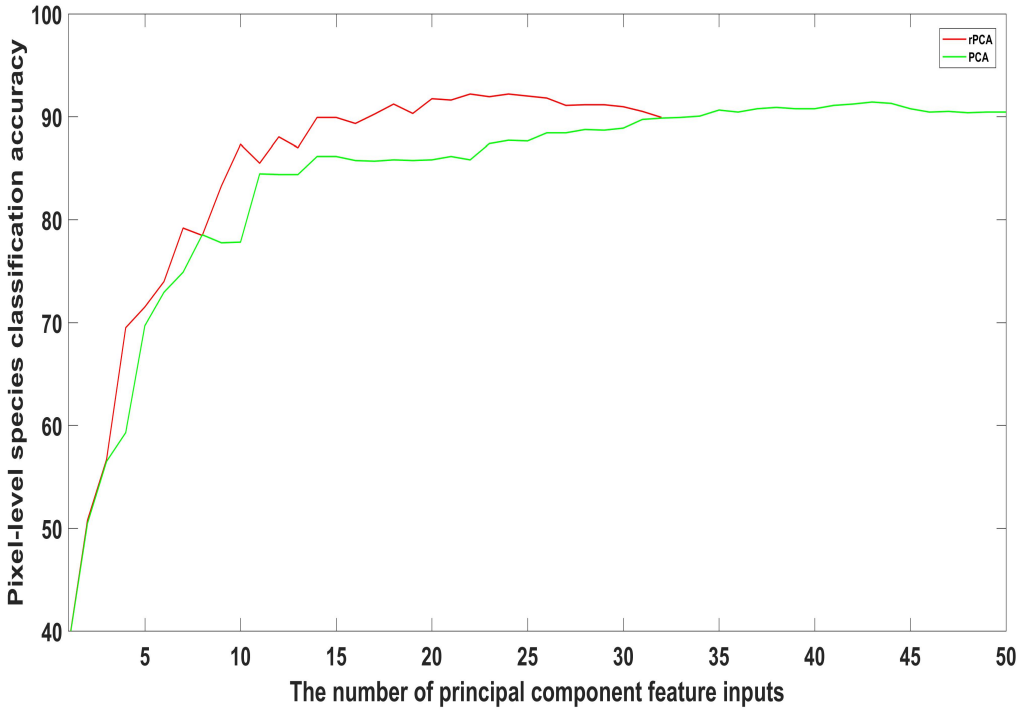

Fig. 8. The pixel-level classification accuracy with respect to the number of principal component feature inputs

temperate forest. Our pixel-level species classification method showed that 89% of pixels were correctly assigned overall. The overall accuracy of ITC-level tree species classification was 65.8%. The low accuracy at the ITC-level classification might be related to inaccurate geopositioning of the ground truth dataset because visual analysis showed that species distribution patterns agreed well with ground truth. Further study is required to evaluate our method with accurately georeferenced ground truth data. Nonetheless, this study shows the potential of rPCA and machine learning approaches to distinguish species using hyperspectral imagery.

VII. Acknowledgements

This project is supported by a grant from DEFRA / BBSRC to study the spread of ash dieback in British woodlands. The authors would like to thank NERC-ARSF for collecting and pre-processing the data used in this research project [RG13/08/175b], and a grant from the Isaac Newton Trust.

References

[1] G. Asner, D. Knapp, A. Balaji, and G. Páez-Acosta, "Automated mapping of tropical deforestation and forest degradation: Claslite," *Journal of Applied Remote Sensing*, vol. 3, no. 1, pp. 033 543–033 543, 2009.

[2] R. Houghton, K. Lawrence, J. Hackler, and S. Brown, "The spatial distribution of forest biomass in the brazilian amazon: a comparison of estimates," *Global Change Biology*, vol. 7, no. 7, pp. 731–746, 2001.

[3] Z. A. Latif, I. Zamri, and H. Omar, "Determination of tree species using worldview-2 data," in *Signal Processing and its Applications (CSPA), 2012 IEEE 8th International Colloquium on*. IEEE, 2012, pp. 383–387.

[4] M. Immitzer, C. Atzberger, and T. Koukal, "Tree species classification with random forest using very high spatial resolution 8-band worldview-2 satellite data," *Remote Sensing*, vol. 4, no. 9, pp. 2661–2693, 2012.

[5] K. Y. Peerbhay, O. Mutanga, and R. Ismail, "Investigating the capability of few strategically placed worldview-2 multispectral bands to discriminate forest species in kwazulu-natal, south africa," *Selected Topics in Applied Earth Observations and Remote Sensing, IEEE Journal of*, vol. 7, no. 1, pp. 307–316, 2014.

[6] G. Omer, O. Mutanga, E. M. Abdel-Rahman, and E. Adam, "Performance of support vector machines and artificial neural network for mapping endangered tree species using worldview-2 data in dukuduku forest, south africa," *Selected Topics in Applied Earth Observations and Remote Sensing, IEEE Journal of*, 2015.

[7] G. P. Asner, R. E. Martin, A. J. Ford, D. J. Metcalfe, and M. J. Liddell, "Leaf chemical and spectral diversity in australian tropical forests," *Ecological Applications*, vol. 19, no. 1, pp. 236–253, 2009.

[8] J.-B. Féret and G. P. Asner, "Spectroscopic classification of tropical forest species using radiative transfer modeling," *Remote Sensing of Environment*, vol. 115, no. 9, pp. 2415–2422, 2011.

[9] ——, "Tree species discrimination in tropical forests using airborne imaging spectroscopy," *Geoscience and Remote Sensing, IEEE Transactions on*, vol. 51, no. 1, pp. 73–84, 2013.

[10] G. P. Asner, "Biophysical and biochemical sources of variability in canopy reflectance," *Remote sensing of Environment*, vol. 64, no. 3, pp. 234–253, 1998.

[11] M. Cochrane, "Using vegetation reflectance variability for species level classification of hyperspectral data," *International Journal of Remote Sensing*, vol. 21, no. 10, pp. 2075–2087, 2000.

[12] K. L. Castro-Esau, G. A. Sánchez-Azofeifa, B. Rivard, S. J. Wright, and M. Quesada, "Variability in leaf optical properties of mesoamerican trees and the potential for species classification," *American Journal of Botany*, vol. 93, no. 4, pp. 517–530, 2006.

[13] G. Asner, J. Boardman, C. Field, D. Knapp, T. Kennedy-Bowdoin, M. Jones, and R. Martin, "Carnegie airborne observatory: in-flight fusion of hyperspectral imaging and waveform light detection and ranging for three-dimensional studies of ecosystems," *Journal of Applied Remote Sensing*, vol. 1, no. 1, pp. 013 536–013 536, 2007.

[14] M. L. Clark, D. A. Roberts, and D. B. Clark, "Hyperspectral discrimination of tropical rain forest tree species at leaf to crown scales," *Remote sensing of environment*, vol. 96, no. 3, pp. 375–398, 2005.

[15] J. Zhang, B. Rivard, A. Sánchez-Azofeifa, and K. Castro-Esau, "Intra- and inter-class spectral variability of tropical tree species at la selva, costa rica: Implications for species identification using hydice imagery," *Remote Sensing of Environment*, vol. 105, no. 2, pp. 129–141, 2006.

[16] M. A. Cho, P. Debba, R. Mathieu, L. Naidoo, J. Van Aardt, and G. P. Asner, "Improving discrimination of savanna tree species through a multiple-endmember spectral angle mapper approach: Canopy-level analysis," *Geoscience and Remote Sensing, IEEE Transactions on*, vol. 48, no. 11, pp. 4133–4142, 2010.

[17] C. A. Baldeck and G. P. Asner, "Single-species detection with airborne imaging spectroscopy data: A comparison of support vector techniques," *Selected Topics in Applied Earth Observations and Remote Sensing, IEEE Journal of*, vol. 8, no. 6, pp. 2501–2512, 2015.

[18] M. Dalponte, L. Bruzzone, L. Vescovo, and D. Gianelle, "The role of spectral resolution and classifier complexity in the analysis of hyperspectral images of forest areas," *Remote Sensing of Environment*, vol. 113, no. 11, pp. 2345–2355, 2009.

[19] K. M. Dahlin, G. P. Asner, and C. B. Field, "Environmental and community controls on plant canopy chemistry in a mediterranean-type ecosystem," *Proceedings of the National Academy of Sciences*, vol. 110, no. 17, pp. 6895–6900, 2013.

[20] N. Goodwin, R. Turner, and R. Merton, "Classifying eucalyptus forests with high spatial and spectral resolution imagery: an investigation of individual species and vegetation communities," *Australian Journal of Botany*, vol. 53, no. 4, pp. 337–345, 2005.

[21] R. Hill, A. Wilson, M. George, and S. Hinsley, "Mapping tree species in temperate deciduous woodland using time-series multi-spectral data," *Applied Vegetation Science*, vol. 13, no. 1, pp. 86–99, 2010.

[22] T. Matsuki, N. Yokoya, and A. Iwasaki, "Hyperspectral tree species classification of japanese complex mixed forest with the aid of lidar data," *Selected Topics in Applied Earth Observations and Remote Sensing, IEEE Journal of*, vol. 8, no. 5, pp. 2177–2187, 2015.

[23] M. Dalponte, H. O. Orka, T. Gobakken, D. Gianelle, and E. Næsset, "Tree species classification in boreal forests with hyperspectral data," *Geoscience and Remote Sensing, IEEE Transactions on*, vol. 51, no. 5, pp. 2632–2645, 2013.

[24] M. Dalponte, L. T. Ene, H. O. Orka, T. Gobakken, and E. Naesset, "Unsupervised selection of training samples for tree species classification using hyperspectral data," *Selected Topics in Applied Earth Observations and Remote Sensing, IEEE Journal of*, vol. 7, no. 8, pp. 3560–3569, 2014.

[25] M. Colgan, C. B. adn J. Féret, and G. Asner, "Mapping savanna tree species at ecosystem scales using support vector machine classification and brdf correction on airborne hyperspectral and lidar data," *Remote Sensing*, vol. 4, no. 11, pp. 3462–3480, 2012.

[26] M. Dalponte, L. Bruzzone, and D. Gianelle, "Fusion of hyperspectral and lidar remote sensing data for classification of complex forest areas," *Geoscience and Remote Sensing, IEEE Transactions on*, vol. 46, no. 5, pp. 1416–1427, 2008.

[27] T. G. Jones, N. C. Coops, and T. Sharma, "Assessing the utility of airborne hyperspectral and lidar data for species distribution mapping in the coastal pacific northwest, canada," *Remote Sensing of Environment*, vol. 114, no. 12, pp. 2841–2852, 2010.

[28] M. Dalponte, L. Bruzzone, and D. Gianelle, "Tree species classification in the southern alps based on the fusion of very high geometrical resolution multispectral/hyperspectral images and lidar data," *Remote sensing of environment*, vol. 123, pp. 258–270, 2012.

[29] A. Ghosh, F. E. Fassnacht, P. Joshi, and B. Koch, "A framework for mapping tree species combining hyperspectral and lidar data: Role of selected classifiers and sensor across three spatial scales," *International Journal of Applied Earth Observation and Geoinformation*, vol. 26, pp. 49–63, 2014.

[30] Q. Chen, D. Baldocchi, P. Gong, and M. Kelly, "Isolating individual trees in a savanna woodland using small footprint lidar data," *Photogrammetric Engineering and Remote Sensing*, vol. 72, no. 8, pp. 923–932, 2006.

[31] J. Heinzel and B. Koch, "Investigating multiple data sources for tree species classification in temperate forest and use for single tree delineation," *International Journal of Applied Earth Observation and Geoinformation*, vol. 18, pp. 101–110, 2012.

[32] C. Zhang and F. Qiu, "Mapping individual tree species in an urban forest using airborne lidar data and hyperspectral imagery," *Photogrammetric Engineering & Remote Sensing*, vol. 78, no. 10, pp. 1079–1087, 2012.

[33] M. Voss and R. Sugumaran, "Seasonal effect on tree species classification in an urban environment using hyperspectral data, lidar, and an object-oriented approach," *Sensors*, vol. 8, no. 5, pp. 3020–3036, 2008.

[34] M. Alonzo, B. Bookhagen, and D. A. Roberts, "Urban tree species mapping using hyperspectral and lidar data fusion," *Remote Sensing of Environment*, vol. 148, pp. 70–83, 2014.

[35] M. Dalponte, H. O. Ørka, L. T. Ene, T. Gobakken, and E. Næsset, "Tree crown delineation and tree species classification in boreal forests using hyperspectral and als data," *Remote sensing of environment*, vol. 140, pp. 306–317, 2014.

[36] C. Iovan, D. Boldo, and M. Cord, "Detection, characterization, and modeling vegetation in urban areas from high-resolution aerial imagery," *Selected Topics in Applied Earth Observations and Remote Sensing, IEEE Journal of*, vol. 1, no. 3, pp. 206–213, 2008.

[37] R. Dinuls, G. Erins, A. Lorencs, I. Mednieks, and J. Sinica-Sinavskis, "Tree species identification in mixed baltic forest using lidar and multispectral data," *Selected Topics in Applied Earth Observations and Remote Sensing, IEEE Journal of*, vol. 5, no. 2, pp. 594–603, 2012.

[38] J. Lee, X. Cai, C.-B. Schölieb, and D. Coomes, "Nonparametric image registration of airborne lidar, hyperspectral and photographic imagery of wooded landscapes," *Geoscience and Remote Sensing, IEEE Transactions on*, in press.

[39] A. Persson, J. Holmgren, and U. Söderman, "Detecting and measuring individual trees using an airborne laser scanner," *Photogrammetric Engineering and Remote Sensing*, vol. 68, no. 9, pp. 925–932, 2002.

[40] J. Lee, X. Cai, J. Lellmann, C.-B. Schönlieb, and D. Coomes, "3d individual tree segmentation from fully integrated lidar, hyperspectral imagery and aerial photographs," *Technical report, DAMTP, Cambridge*, 2015.

[41] E. J. Candès, X. Li, Y. Ma, and J. Wright, "Robust principal component analysis?" *Journal of the ACM (JACM)*, vol. 58, no. 3, p. 11, 2011.

[42] C.-C. Chang and C.-J. Lin, "LIBSVM: A library for support vector machines," *ACM Transactions on Intelligent Systems and Technology*, vol. 2, pp. 27:1–27:27, 2011, software available at http://www.csie.ntu.edu.tw/~cjlin/libsvm.

[43] N. Butt, G. Campbell, Y. Malhi, M. Morecroft, K. Fenn, and M. Thomas, "Initial results from establishment of a long-term broadleaf monitoring plot at wytham woods, oxford, uk," *University*

of Oxford Report, 2009. [Online]. Available: http://ctfs.si.edu/Public/plotdataaccess/TermsConditions.php?plotid=30&typedata=tree

[44] J. P. Hoffbeck, D. Landgrebe *et al.*, "Effect of radiance-to-reflectance transformation and atmosphere removal on maximum likelihood classification accuracy of high-dimensional remote sensing data," in *Geoscience and Remote Sensing Symposium, 1994. IGARSS'94. Surface and Atmospheric Remote Sensing: Technologies, Data Analysis and Interpretation., International*, vol. 4. IEEE, 1994, pp. 2538–2540.

[45] H.-R. Y. Sun-Hwa Kim, Jung-Il Shin and K.-S. Lee, "Effect of atmospheric correction for the land cover classification using hyperspectral data," *Proceeding of 2006 Asian Conference on Remote Sensing*, 2006.

[46] I. Jolliffe, *Principal component analysis*. Wiley Online Library, 2002.

[47] X. Yuan and J. Yang, "Sparse and low-rank matrix decomposition via alternating direction methods," *preprint*, 2009.

[48] H. Hu, J. Feng, C. Yu, and J. Zhou, "Multi-class constrained normalized cut with hard, soft, unary and pairwise priors and its applications to object segmentation," *Image Processing, IEEE Transactions on*, vol. 22, no. 11, pp. 4328–4340, 2013.

[49] J.-B. Féret and G. P. Asner, "Semi-supervised methods to identify individual crowns of lowland tropical canopy species using imaging spectroscopy and lidar," *Remote Sensing*, vol. 4, no. 8, pp. 2457–2476, 2012.

[50] F. E. Fassnacht, C. Neumann, M. Forster, H. Buddenbaum, A. Ghosh, A. Clasen, P. K. Joshi, and B. Koch, "Comparison of feature reduction algorithms for classifying tree species with hyperspectral data on three central european test sites," *Selected Topics in Applied Earth Observations and Remote Sensing, IEEE Journal of*, vol. 7, no. 6, pp. 2547–2561, 2014.

[51] R. G. Pontius Jr and M. Millones, "Death to kappa: birth of quantity disagreement and allocation disagreement for accuracy assessment," *International Journal of Remote Sensing*, vol. 32, no. 15, pp. 4407–4429, 2011.

[52] NEWFOR, "Alpine space programme, european territorial cooperation 2007-2013-project newfor," 2012. [Online]. Available: http://www.newfor.net/projet/

[53] L. Eysn, M. Hollaus, E. Lindberg, F. Berger, J.-M. Monnet, M. Dalponte, M. Kobal, M. Pellegrini, E. Lingua, D. Mongus *et al.*, "A benchmark of lidar-based single tree detection methods using heterogeneous forest data from the alpine space," *Forests*, vol. 6, no. 5, pp. 1721–1747, 2015.

[54] E. Puttonen, P. Litkey, and J. Hyyppä, "Individual tree species classification by illuminated–shaded area separation," *Remote Sensing*, vol. 2, no. 1, pp. 19–35, 2009.

[55] G. Tochon, J. Féret, S. Valero, R. Martin, D. Knapp, P. Salembier, J. Chanussot, and G. Asner, "On the use of binary partition trees for the tree crown segmentation of tropical rainforest hyperspectral images," *Remote Sensing of Environment*, vol. 159, pp. 318–331, 2015.

[56] C. A. Baldeck and G. P. Asner, "Improving remote species identification through efficient training data collection," *Remote Sensing*, vol. 6, no. 4, pp. 2682–2698, 2014.

Juheon Lee Juheon Lee received the BA degree from Seoul National University, South Korea, and the MPhil in Atmospheric Science, University of Cambridge, U.K., in 2010 and 2012, respectively. Since 2012, he has been with the Department of Applied Mathematics and Theoretical Physics (DAMTP), and Plant Sciences, University of Cambridge. He is currently working toward the Ph.D. degree in the Department of Plant Sciences, University of Cambridge, Cambridge, U.K. His research interests include image processing and its application to geophysics, remote sensing and biomedical imaging.

Xiaohao Cai Xiaohao Cai received the M.S. degree in mathematics from Zhejiang University, China, in 2008, and the Ph.D. degree in mathematics from The Chinese University of Hong Kong, Hong Kong in 2012.

He is currently a postdoctoral researcher in Mullard Space Science Laboratory of University College London (UCL). He was a postdoctoral researcher in the Department of Plant Sciences, and Department of Applied Mathematics and Theoretical Physics, University of Cambridge, during May 2014 – Dec. 2016, and in the University of Kaiserslautern, during Sep. 2012 – May 2014. His research interests include image processing, numerical analysis and their applications in medical imaging, remote sensing, and radio interferometry, just to name a few.

Jan Lellmann Jan Lellmann is a professor in Applied Mathematics at the Institute for Mathematics and Image Computing, University of Lbeck. Jan obtained degrees in Computer Science and Mathematics from Heidelberg University in 2006 and 2007, and his doctoral degree from University of Heidelberg in 2011. After spending four years as a post-doctoral researcher and Leverhulme Early Career Fellow in the Cambridge Image Analysis group, University of Cambridge, he became full professor at the University of Lbeck in 2015. Jan's work focuses on modelling application-specific prior knowledge in image processing, in order to develop methods that are more accurate and require less data. He is particularly interested in high-dimensional problems that are non-differentiable, or where a number of discrete decisions has to be made, such as the image segmentation problem. Application areas include processing and analysis of images, videos, as well as general two- and higher-dimensional data, such as directional, tensor-, or height data in medicine, biology, and earth sciences.

Michele Dalponte Michele Dalponte received the M.Sc. degree in Telecommunications Engineering, and the PhD in Information and Communication Technologies from the University of Trento, Italy in 2006 and 2010, respectively. He worked as Post-doctoral Researcher at the Norwegian University of Life Sciences (Norway) and at the University of Cambridge (UK). He is currently Researcher at the Forest Ecology and Biogeochemical Cycles Group at the Research and Innovation Center of the Edmund Mach Foundation (Italy). His research interests are in the field of remote sensing, in particular the analysis of hyperspectral, multispectral and LIDAR data for forest monitoring. His work has been published in international journals and presented at international conferences. He is a reviewer for many remote sensing journals.

Yadvinder Malhi Yadvinder Malhi is Professor of Ecosystem Science at Oxford University. His research interests include the dynamics and physiology of forests and how they respond to change. He maintains the 18 ha plot at Wytham Woods that is the focus of this study.

Nathalie Butt Nathalie Butt is an Australian Research Council Fellow in the Centre of Excellence for Environmental Decisions at the University of Queensland. She works at the interface of climate and ecosystem science. Research themes include the vulnerability of species and ecosystems to climate change, and forest response and biophysical feedbacks to land cover change.

PLACE PHOTO HERE

Mike Morecroft Mike Morecroft is an environmental scientist working for the nature conservation agency for England.

Carola-Bibiane Schönlieb Carola-Bibiane Schnlieb is a Reader in Applied and Computational Analysis, head of the Cambridge Image Analysis (CIA) group at the Department of Applied Mathematics and Theoretical Physics (DAMTP), University of Cambridge. Moreover, she is the Director of the Cantab Capital Institute for the Mathematics of Information, Co-Director of the EPSRC Centre for Mathematical and Statistical Analysis of Multimodal Clinical Imaging, a Fellow of Jesus College, Cambridge and co-leader of the IMAGES network. Carola obtained her degree in Mathematics at the University of Salzburg in 2004 and her Ph.D. in Mathematics at the University of Cambridge in 2009. After one year of postdoctoral activity at the University of Gttingen (Germany), she became a Lecturer in DAMTP, promoted to Reader in 2015. She is an internationally-acknowledged researcher in applied and computational mathematics with particular focus on variational methods for image analysis and image reconstruction, including work on biomedical imaging, remote sensing and image inpainting. She has active interdisciplinary collaborations with clinicians, biologists, physicists, art conservators, chemical engineers and plant scientists.

David Coomes David A. Coomes joined the staff of the Plant Sciences Department of Cambridge University in 2000. He is head of the Forest Ecology and Conservation Group. His current interests research include modeling the impacts of anthropogenic global change using large-scale forest inventories, and developing approaches for mapping forest change using airborne remote sensing technologies.